CLASSIC: Consistent Longitudinal Alignment and Segmentation for Serial Image Computing

Zhong Xue, Dinggang Shen, and Christos Davatzikos

Section of Biomedical Image Analysis, Department of Radiology,
University of Pennsylvania, Philadelphia, PA 19104
{zhong.xue, dinggang.shen, christos.davatzikos}@uphs.upenn.edu

Abstract. This paper proposes a temporally-consistent and spatially-adaptive longitudinal MR brain image segmentation algorithm, referred to as CLASSIC, which aims at obtaining accurate measurements of rates of change of regional and global brain volumes from serial MR images. The algorithm incorporates image-adaptive clustering, spatiotemporal smoothness constraints, and image warping to jointly segment a series of 3-D MR brain images of the same subject that might be undergoing changes due to development, aging or disease. Morphological changes, such as growth or atrophy, are also estimated as part of the algorithm. Experimental results on simulated and real longitudinal MR brain images show both segmentation accuracy and longitudinal consistency.

1 Introduction

MR brain image segmentation is a key processing step in many brain image analysis applications, *e.g.* morphometry, automatic tissue labeling, tissue volume quantification, image registration, and computer integrated surgery [1, 2, 3, 4, 5, 6, 7, 8]. Analysis of a series of 3-D data of the same subject captured at different time-points, *i.e.* of a 4-D image, is important in many neuroimaging studies that concentrate on normal development, aging, and evolution of pathology [9]. Consistent segmentation is particularly important in the literature of aging and Alzheimer's Disease (AD) since subtle brain changes that might be indicative of early stages of underlying pathology must be estimated from serial MR images. However, existing 3-D segmentation algorithms may not provide adequate longitudinal stability for serial brain images since they process each image at a time. Herein, we propose a 4-D segmentation method that overcomes this limitation and significantly improves longitudinal stability of segmentation.

Fuzzy algorithms [1, 2, 3, 4, 5, 10] have been proven to be more suitable for 3-D MR images than hard segmentation algorithms since the intensity of each voxel of an MR image may represent a combination of different tissues. Fuzzy C-Means (FCM) algorithms have been used in many segmentation applications often accounting for intensity inhomogeneity [6, 7, 11, 12] and incorporating spatial information among voxels [8, 13, 14]. The intensity inhomogeneity can be well modeled by the product of the original image and a gain field [12] or by the summation of

G.E. Christensen and M. Sonka (Eds.): IPMI 2005, LNCS 3565, pp. 101–113, 2005.

them [6]. It is also desirable that the clustering algorithm be spatially-adaptive to relatively local image intensity variations in order to adaptively segment tissues of different structures. Different methods have been proposed to incorporate the spatial image context information, including the methods using smoothness constraints of the spatially varying centroid [8], using intensity dissimilarities of neighboring voxels [13], and using smoothing operations of fuzzy membership functions [14]. By combining [6] and [14], Pham and Prince proposed a Fuzzy And Noise Tolerant Adaptive Segmentation Method (FANTASM), which is robust to the effects of both intensity inhomogeneities and noise, while providing a soft segmentation [http://iacl.ece.jhu.edu/projects/fantasm/]. The advantage of FANTASM is that it uses the intermediate information of the segmentation results while compensating the gain field and performing smoothness on the membership functions. However, in FANTASM, the spatial smoothness constraints of fuzzy membership functions are the same for all the locations in an image, which can result in an "over smoothing" effect across tissue boundaries. More importantly, FANTASM and other existing segmentation methods are designed for segmentation of 3-D images, and they might yield inconsistent results when applied to serial scans of the same subject, thereby rendering estimations of rates of brain atrophy and growth noisy.

In this paper, we propose a novel algorithm for longitudinal MR brain image segmentation based on FANTASM, which we refer to as CLASSIC (Consistent Longitudinal Alignment and Segmentation for Serial Image Computing). CLASSIC not only jointly segments longitudinal 3-D MR brain images of the same subject, but also estimates the longitudinal deformations in the image series, *e.g.* tissue atrophy. It iteratively performs two steps: *(1)* it jointly segments serial 3-D images using a 4-D image-adaptive clustering algorithm based on the current estimate of the longitudinal deformations in the image series, *(2)* it then refines these longitudinal deformations using a 4-D elastic warping algorithm [15, 16]. In this way, we obtain both a longitudinally-consistent segmentation result and an estimate of longitudinal deformation of anatomy in a series of 3-D images. The 4-D image-adaptive clustering algorithm used in CLASSIC extends FANTASM in three aspects. First, a new temporal consistency constraint term on the fuzzy membership functions is used in order to obtain temporally-consistent segmentation results. Second, the spatiotemporal constraints of fuzzy membership functions are made adaptive to the smoothness of the image, *i.e.* they are stronger in the regions that have more uniform image intensities, and vice versa, thus fuzzy membership functions are not necessarily overly smooth across tissue boundaries. Third, the clustering centers at each voxel location are adaptive to local image intensity variations. In this way, the proposed algorithm not only provides temporally-consistent segmentation results, but also adapts to local image intensity variations.

Experiments are performed to segment simulated and real longitudinal MR brain images. The longitudinal 3-D T1-SPGR MR images of healthy, older adults from the Baltimore Longitudinal Study of Aging (BLSA) [9] are used in the experiments, which display both brain atrophy and changes of tissue contrast due

to vascular and possibly other pathologies. In all the experiments, we focused on evaluating the performance of the CLASSIC and FANTASM algorithms in terms of obtaining temporally-consistent segmentation, capturing global and local intensity/contrast changes, as well as estimating longitudinal deformations. The results demonstrate that CLASSIC gives consistent segmentation results across different years and adapts to image intensity variations.

2 Serial Image Segmentation

2.1 The Framework of CLASSIC

A 4-D MR brain image in the context of this work is a series of 3-D MR brain images obtained from the same subject at different times. Because the brain changes that we might be interested in can be extremely small, for example in early stages of Alzheimer's Disease (AD), temporally-inconsistent segmentation can significantly reduce the statistical power of longitudinal neuroimaging studies aiming at determining early structural changes as markers of AD. In this paper, we focus on jointly segmenting a 4-D image and follow the underlying temporal changes in anatomical structures, in order to provide more stable and consistent tissue segmentation across different years. Our idea is to classify the tissue of each voxel according to the intensities around that voxel, plus incorporating image-adaptive spatiotemporal constraints at that location. Therefore, a 4-D image segmentation framework, referred to as CLASSIC, is proposed, which iteratively performs the following two steps: *(1)* given a current estimate of the longitudinal deformations necessary to align 3-D images, it jointly segments the image series using a 4-D image-adaptive clustering algorithm, *(2)* it then refines the longitudinal deformations using a 4-D HAMMER registration algorithm [15].

The pre-processing of the input 3-D image series include: correct global intensity inhomogeneity [6] and globally normalize the intensities of each image according to the histogram of the first image [17]; transfer the subsequent images onto the space of the first image using rigid transformations. After preprocessing, CLASSIC is applied to consistently segment the rigidly aligned serial images $I_t, t \in T = \{t_1, t_2, ..., t_Y\}$, with initial longitudinal deformations from the first image I_{t_1} to other images I_t as $F_{t_1 \to t}$, $t = t_2, t_3, ..., t_Y$, and Y being the total number of the serial images. If no initial longitudinal deformations among the images are available, $F_{t_1 \to t}(i) = 0$, where i refers to a voxel location in the first image I_{t_1}, *i.e.* initially there is no deformation at all. The standard FCM algorithm is also performed on each image I_t to give initial values of the clustering centroids. Then, CLASSIC iteratively performs the following two steps:

1. Apply the proposed 4-D image-adaptive clustering algorithm to the image series $I_t, t \in T$, based on the current estimate of the longitudinal deformations $F_{t_1 \to t}$, $t = t_2, t_3, ..., t_Y$, and obtain the segmented images $I_t^{(\text{seg})}, t \in T$ (The algorithm will be described in Section 2.2 in detail).
2. Use the 4-D HAMMER [15], to register the segmented images $I_t^{(\text{seg})}$, $t = \{t_2, t_3, ..., t_Y\}$ onto the reference image series formed by repeating the first

segmented image $I_{t_1}^{\text{seg}}$ for $Y-1$ times, *i.e.* $I_{t_1}^{(\text{seg})}, I_{t_1}^{(\text{seg})}, ..., I_{t_1}^{(\text{seg})}$. After performing 4-D registration, the longitudinal deformations $F_{t_1 \to t}, t = t_2, t_3, ..., t_Y$ are refined according to the 4-D segmentation results of step (1). Go to step (1) if the amount of deformation changes between two iterations is larger than a prescribed threshold; otherwise terminate with $I_t^{(\text{seg})}$ and $F_{t_1 \to t}$ as the final segmentation results and the final estimate of the longitudinal deformations, respectively.

These two steps are performed iteratively so that consistent segmentation results can be obtained. In practice, we find that a few iterations are enough to obtain stable segmentation results. In Section 2.2, we describe the 4-D image-adaptive clustering algorithm used in step (1) of CLASSIC in detail.

2.2 The 4-D Image-Adaptive Clustering Algorithm

Algorithm Formulation. Given image series $I_t, t \in T$ and the longitudinal deformations $F_{t_1 \to t}, t = t_2, ..., t_Y$, the purpose of the 4-D segmentation is to calculate the segmented images $I_t^{(\text{seg})}, t \in T$. Since $F_{t_1 \to t}$ is the deformation from I_{t_1} to I_t, the corresponding point of voxel i of image I_{t_1} will be $F_{t_1 \to t}(i)$ in image I_t. For simplicity, we denote point $F_{t_1 \to t}(i)$ in image I_t as (t, i), and $x_{(t,i)}$ as its intensity. According to the 4-D image-adaptive clustering algorithm, $x_{(t,i)}(t \in T, i \in \Omega)$ is classified into different tissue types by finding $c_{(t,i),k}$, the kth clustering center at location (t, i), and $\mu_{(t,i),k}$, the fuzzy membership function of $x_{(t,i)}$ belonging to class k, and by minimizing the objective function in Eq.(1), which includes three terms: the weighted squared error between the intensities around each voxel and the clustering centroids, the spatially-adaptive smoothness constraints, and temporally-adaptive smoothness constraints.

$$\begin{aligned} E(\mu, c) = & \sum_{t \in T} \sum_{i \in \Omega} \{ \frac{1}{S(N_{(t,i)})} \sum_{k=1}^{K} \sum_{(\tau,j) \in N_{(t,i)}} [\mu_{(\tau,j),k}^{q} (x_{(\tau,j)} - c_{(t,i),k})^2] \} \\ & + \frac{\alpha}{2} \sum_{t \in T} \sum_{i \in \Omega} \{ \rho_{(t,i)}^{(s)} \sum_{k=1}^{K} [\mu_{(t,i),k}^{q} \bar{\mu}_{(t,i),k}^{(s)}] \} \\ & + \frac{\beta}{2} \sum_{t \in T} \sum_{i \in \Omega} \{ \rho_{(t,i)}^{(t)} \sum_{k=1}^{K} [\mu_{(t,i),k}^{q} \bar{\mu}_{(t,i),k}^{(t)}] \}, \end{aligned} \tag{1}$$

where $\bar{\mu}_{(t,i),k}^{(s)} = \frac{1}{N_1} \sum_{(t,j) \in N_{(t,i)}^{(s)\prime}} \sum_{m \in M_k} \mu_{(t,j),m}^{q}$, $\bar{\mu}_{(t,i),k}^{(t)} = \frac{1}{N_2} \sum_{(\tau,i) \in N_{(t,i)}^{(t)\prime}} \sum_{m \in M_k} \mu_{(\tau,i),m}^{q}$.

The fuzzy membership functions are subject to

$$\sum_{k=1}^{K} \mu_{(t,i),k} = 1, \text{ for all } i \in \Omega, t \in T. \tag{2}$$

In Eq.(1), $N_{(t,i)}$ is the spatiotemporal neighborhood of point (t, i). It is a combination of its spatial neighborhood $N_{(t,i)}^{(s)}$ and temporal neighborhood $N_{(t,i)}^{(t)} =$

$\{(\tau, i) : |\tau - t| \leq T_N\}$, thus $N_{(t,i)} = N^{(s)}_{(t,i)} \cup N^{(t)}_{(t,i)}$. $S(N_{(t,i)})$ represents the number of voxels within $N_{(t,i)}$. In the first term of Eq.(1), the centroids $c_{(t,i),k}$ are adaptively changed at different image locations based on local image intensity variations within the spatiotemporal neighborhood $N_{(t,i)}$ of each location. The second term of Eq.(1) reflects the spatial constraints of the fuzzy membership functions, which is analogous to the FANTASM algorithm. The difference is that an additional factor $\rho^{(s)}_{(t,i)}$ is used as an image-adaptive weighting coefficient, thus stronger smoothness constraints are applied to the fuzzy membership functions in the image regions that have more uniform intensities, and vice versa. The third term of Eq.(1) reflects the temporal consistency constraints. Similar to $\rho^{(s)}_{(t,i)}$, $\rho^{(t)}_{(t,i)}$ is a weighting coefficient that reflects the temporal smoothness of the image. $\bar{\mu}^{(s)}_{(t,i),k}$ and $\bar{\mu}^{(t)}_{(t,i),k}$ are the means of $\mu^q_{(\tau,l),k}$ in the spatial and temporal neighborhoods $N^{(s)'}_{(t,i)}$ and $N^{(t)'}_{(t,i)}$ of the current position (t, i), respectively ($N^{(s)'}_{(t,i)}$ and $N^{(t)'}_{(t,i)}$ do not include the point (t, i)). α and β are the weighting coefficients and N_1 and N_2 are the numbers of addends for normalization.

$\rho^{(s)}_{(t,i)}$ is the spatial smoothness factor of image I_t at voxel (t, i). The value of $\rho^{(s)}_{(t,i)}$ is close to 1 when the image around voxel (t, i) is spatially-smooth, and close to 0 when the image around voxel (t, i) is not spatially-smooth. Using a spatial difference operator D_r along each of 3 spatial axis r, $\rho^{(s)}_{(t,i)}$ is defined as

$$\rho^{(s)}_{(t,i)} = \exp\{-\sum_r [(D_r * I_t)^2_{(t,i)}/2\sigma_s^2]\}, \tag{3}$$

where $(D_r * I_t)_{(t,i)}$ refers to first calculating the spatial convolution $(D_r * I_t)$, and then taking its value at location (t, i). $\rho^{(t)}_{(t,i)}$ is the temporal smoothness factor,

$$\rho^{(t)}_{(t,i)} = \exp\{-(D_t * x_{(t,i)})^2_t/2\sigma_t^2\}, \tag{4}$$

where D_t is the temporal difference operator, and $(D_t * x_{(t,i)})_t$ refers to first calculating the temporal convolution $(D_t * x_{(t,i)})$ and then taking its value at t.

Notice the size of the spatiotemporal neighborhood $N_{(t,i)}$ at each location (t, i) can also be adaptively adjusted. A smaller neighborhood size will make the algorithm much adaptive to local image intensity variations, while a larger neighborhood size has to be used to capture adequate intensity information of different tissues around that location in order to label that voxel correctly. No spatiotemporal smoothness constraints on c were used in Eq.(1), because we have found that the image-adaptive constraints of μ along with reasonably large and smooth neighborhood sizes are adequate for yielding smoothly varying centroids.

Finding the Solutions of the 4-D Clustering Algorithm. Using Lagrange multipliers to enforce the constraint in Eq.(2), the new objective function is,

$$J = E(\mu, c) + \sum_{t\in T}\sum_{i\in\Omega} \lambda_{(t,i)}(1 - \sum_{k=1}^{K} \mu_{(t,i),k}). \tag{5}$$

Setting the partial derivative of Eq.(5) with respect to $\mu_{(t,i),k}$ to zero, and using Eq.(2), we get the equation to update the fuzzy membership functions,

$$\mu_{(t,i),k} = \frac{[\sum_{(\tau,j)\in\bar{N}_{(t,i)}} \frac{(x_{(t,i)}-c_{(\tau,j),k})^2}{S(N_{(\tau,j)})} + \alpha\rho^{(s)}_{(t,i)}\bar{\mu}^{(s)}_{(t,i),k} + \beta\rho^{(t)}_{(t,i)}\bar{\mu}^{(t)}_{(t,i),k}]^{\frac{-1}{q-1}}}{\sum_{k=1}^{K}[\sum_{(\tau,j)\in\bar{N}_{(t,i)}} \frac{(x_{(t,i)}-c_{(\tau,j),k})^2}{S(N_{(\tau,j)})} + \alpha\rho^{(s)}_{(t,i)}\bar{\mu}^{(s)}_{(t,i),k} + \beta\rho^{(t)}_{(t,i)}\bar{\mu}^{(t)}_{(t,i),k}]^{\frac{-1}{q-1}}}. \tag{6}$$

Since different spatiotemporal neighborhood sizes are used for different image locations, in Eq.(6), $\bar{N}_{(t,i)} = \{(\tau, j) : (t, i) \in N_{(\tau,j)}\}$.

Setting the partial derivative of Eq.(5) with respect to $c_{(t,i),k}$ to zero, the equation to update the centroids can be acquired,

$$c_{(t,i),k} = \frac{\sum_{(\tau,j)\in N_{(t,i)}} \mu^q_{(\tau,j),k} x_{(\tau,j)}}{\sum_{(\tau,j)\in N_{(t,i)}} \mu^q_{(\tau,j),k}}. \tag{7}$$

Given a series of 3-D images and the longitudinal deformations among them, the 4-D image-adaptive clustering algorithm then jointly segments them by iteratively calculating the fuzzy membership functions using Eq.(6) and the centroids using Eq.(7) until convergence. In order to determine adaptively the size of each neighborhood $N_{(t,i)}$, we first initialize an identical neighborhood size for all the locations, and then adaptively adjust these sizes in every iteration: we segment the images using the current fuzzy membership functions, and then calculate the Fractional Anisotropy (FA) [18] of point (t, i) within the current neighborhood $N_{(t,i)}$, denoted as $a_{(t,i)}$. Since FA describes difference proportions of three tissue classes, the size of neighborhood $N_{(t,i)}$ is increased if its $a_{(t,i)}$ is greater than a prescribed threshold a_{high}, or is decreased if $a_{(t,i)}$ is smaller than a threshold a_{low}, or remains unchanged if $a_{(t,i)}$ is between the two thresholds. Finally, the neighborhood sizes are spatially smoothed across the images.

The 4-D image-adaptive clustering algorithm can be summarized as follows:

1. Set α, β, σ_s, σ_t, a_{high}, a_{low} and neighborhoods $N_{(t,i)}$, $N^{(s)'}_{(t,i)}$ and $N^{(t)'}_{(t,i)}$.
2. Compute fuzzy membership functions using Eq.(6).
3. Compute centroids using Eq.(7). In order to accelerate the calculation speed, we only calculate the centroids on down-sampled grid points and linearly interpolate the values at other locations.
4. Segment the images using the current fuzzy membership functions. If the algorithm were converged (the difference of the values of the objective function between two iterations is smaller than a prescribed threshold), then output the segmentation results, otherwise update the size of each spatiotemporal neighborhood $N_{(t,i)}$ and back to step (2).

3 Experimental Results

3.1 Segmentation of Simulated MR Brain Images

In this section, the simulated longitudinal MR brain images are used to evaluate the performance of CLASSIC. Three sets of simulated data are generated,

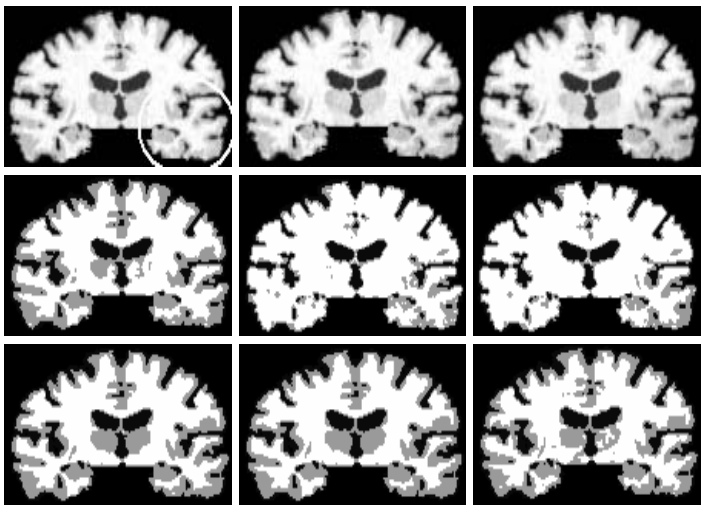

Fig. 1. An example of the segmentation results for simulated 4-D images with local (see the white circle) longitudinal intensity/contrast changes. Top: simulated images, middle: FANTASM results, bottom: CLASSIC results. It can be seen that for FANTASM, because of the intensity and contrast decrease in the spherical region, the overall centroid for WM becomes lower, which results in "over segmentation" of WM

including *(1)* global intensity/contrast decrease; *(2)* local intensity/contrast decrease; and *(3)* local atrophy with intensity/contrast decrease. To generate simulated longitudinal images, starting from a 3-D segmented template image, we set the means of CerebroSpinal Fluid (CSF), Gray Matter (GM) and White Matter (WM) to prescribed intensity values and insert random spatially correlated noise to the image. The initial values of the means of CSF, GM and WM of the first image I_{t_1} were set to 25, 85 and 105, respectively, and the standard deviation of the noise was set to 2. The intensity/contrast decrease is simulated by changing the means of GM and WM (m_g and m_w) with time t. The change rate of GM is defined as $r_g = (m_g(t_Y) - m_g(t_1))/m_g(t_1)/(Y-1)$ and that of WM is defined as $r_w = (m_w(t_Y) - m_w(t_1))/m_w(t_1)(Y-1)$. Different combinations of r_g and r_w yield different simulation results. r_g, r_w, $m_g(t_1)$ and $m_w(t_1)$ determine the change rate of contrast $r_c = (m_w(t_Y) - m_g(t_Y) - m_w(t_1) + m_g(t_1))/(m_w(t_1) - m_g(t_1))/(Y-1)$. Local intensity/contrast changes are achieved by setting r_g and r_w to some values within a prescribed spherical region and setting them to zero outside that region. Gaussian function is used to smooth the change rates across the boundary of this spherical region in order to obtain smooth simulated images. The local atrophy is simulated by matching the Jacobian of the simulated deformation to the desired volumetric changes subject to smoothness and topology preserving constraints [19]. The amount of atrophy can be described by the shrinkage rate, $0 < r_s <= 1$. For example, $r_s = 0.9$ implies a 10% atrophy within the spherical area.

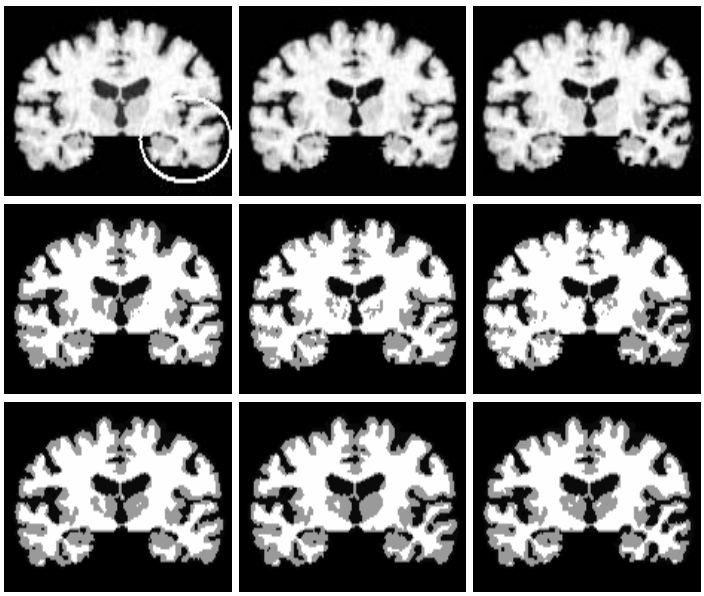

Fig. 2. An example of segmenting the simulated longitudinal data with local atrophy and intensity/contrast decrease. Top: the simulated images, the white circle indicates the spherical area within which atrophy and intensity decrease are simulated, middle: segmentation results of FANTASM, bottom: segmentation results of CLASSIC

CLASSIC and FANTASM were then used to segment these simulated images. In all the experiments, the parameters of CLASSIC were set as follows, $\alpha = 150$, $\beta = 200$, $\sigma_s = 25$, $\sigma_t = 35$, $a_{\text{high}} = 0.3$, $a_{\text{low}} = 0.1$, the initial size of $N^{(s)}_{(t,i)}$ was set to 35 (radius), and $N^{(t)}_{(t,i)}$, $N^{(s)'}_{(t,i)}$ and $N^{(t)'}_{(t,i)}$ were set as the immediate spatial or temporal neighborhoods of (t, i). A quantitative measure of the Correct Classification Rate (CCR) was used to evaluate the similarity between the segmented images and the ground truth. CCR is defined as the percentage of the number of brain voxels that have been correctly labeled according to the ground truth with respect to the total number of brain voxels.

Because of space limitation, we only illustrate some examples of the segmentation results of the simulated images with local intensity/contrast decrease, and with local atrophy. Fig.1 is an example of simulated local intensty/contrast decrease with $r_g = 0$, $r_w = -0.013$ and $r_c = -0.066$. Fig.2 shows an example of simulated local atrophy and intenstiy/contrast decrease, where the shrinkage rate $r_s = 0.8$, and the rates of intensity decrease are $r_g = -0.006$, $r_w = -0.013$, $r_c = -0.035$. The white circles in the images reflect the spherical area within which the atrophy and/or intensity decrease were simulated.

The results of CCR of these two examples are reported in Fig.3 and Fig.4 respectively. Comparing the segmentation results of FANTASM and those of CLASSIC, it can be seen that CLASSIC yields more temporally-consistent seg-

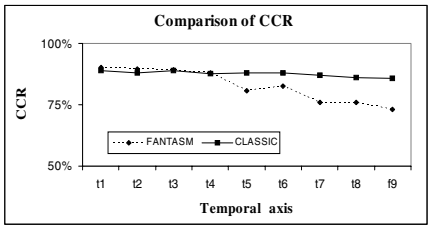

Fig. 3. CCR for the results in Fig.1

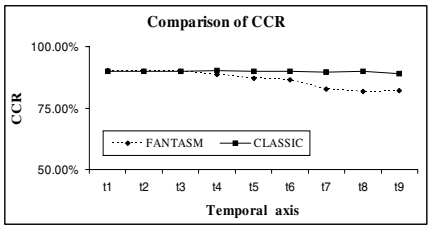

Fig. 4. CCR for the results in Fig.2

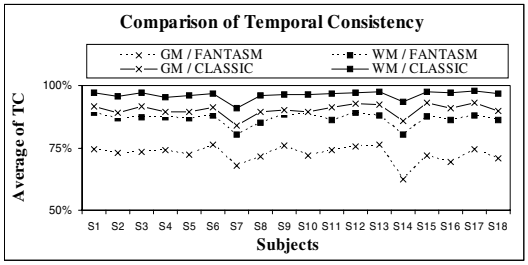

Fig. 5. Temporal consistency of GM and WM of different subjects. Small values indicate relatively less temporally-consistent segmentation

mentation results, while capturing the longitudinal deformations at the same time. Also, comparing either Fig.1 and Fig.2 or Fig.3 and Fig.4, we find that the results of FANTASM in Fig.2 are better than those of Fig.1. This is because their rates of contrast decrease are different. It can also be seen that CLASSIC adapts to local intensity variations quite well. For FANTASM, some larger local intensity variations, *e.g.* contrast decrease, may affect the segmentation results at other image locations. The reason is that FANTASM models the intensity changes through a very smooth gain-field, whereas the 4-D clustering algorithm of CLASSIC is fully-adaptive to local image intensity variations.

3.2 Segmentation of Real Longitudinal MR Brain Images

In this experiment, we used CLASSIC to segment 18 sets of longitudinal MR brain images from the BLSA data [9]. The nine serial scans of each subject were obtained during a period or nine consecutive years. In order to quantitatively analyze the segmentation results, we used a Temporal Consistency (TC) factor to reflect the temporal consistency of the segmentation results. Suppose $x^{\text{seg}}_{(t,i)}$ is the segmentation result (label) of $x_{(t,i)}$, the segmentation results of voxel i across different times can be denoted as $x^{\text{seg}}_{(t_1,i)}$,$x^{\text{seg}}_{(t_2,i)}$,...,$x^{\text{seg}}_{(t_Y,i)}$. Denote L_i as the number of label changes of corresponding voxels across time, then the segmentation of the corresponding voxels is consistent if L_i is small, and vice versa. Therefore, the TC of segmentation results is measured by $TC = 1/S(\Omega') \sum_{i \in \Omega'}(1 - L_i/(Y-1))$,

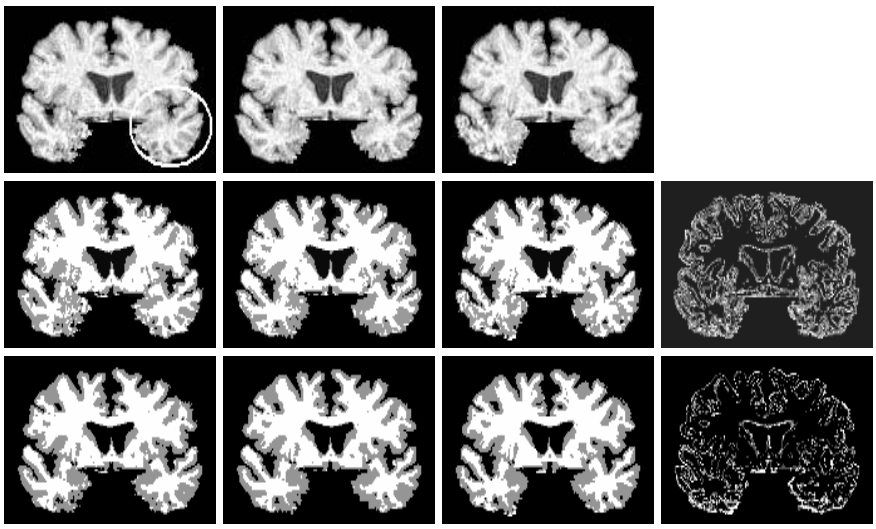

Fig. 6. Comparison of a typical segmentation result of BLSA data using CLASSIC and FANTASM. The top row shows the original serial scans after rigid transformations, the middle row indicates the segmentation results using FANTASM, and the bottom row gives the results of CLASSIC. The two images in the right column show the number of label changes L_i. It can be seen that CLASSIC gives not only spatially-smooth but also temporally-consistent segmentation results. It is worth noting that some atrophy is present between serial scans, thereby contributing to the label changes on the right

where Ω' is the voxel set of the region of interest, and $S(\Omega')$ is the number of voxels in Ω'. Fig.5 gives the TCs of GM and WM of the entire brains calculated from the segmentation results of CLASSIC and FANTASM on the 18 image series respectively. The figure shows that TCs of CLASSIC are much higher than those of FANTASM, which indicates CLASSIC achieves more temporally-consistent results. Fig.6 shows a typical segmentation result using CLASSIC and FANTASM respectively. For comparative purposes, the images shown are the aligned images using rigid transformations. The two images on the right illustrate the number of label changes L_i of corresponding voxels projected on the first image, where white indicates many label changes, and black means no changes across time. In summary CLASSIC got relatively smoother and temporally-consistent segmentation results than FANTASM for real MR image series.

Finally, it is worth noting that although the proposed CLASSIC incorporates temporal smoothness constraints of the segmentation results, it still maintains longitudinal change information. Moreover, CLASSIC captures these changes in a more stable and smooth way by means of the longitudinal deformations among the images and the parameters of the clustering algorithm. For example, Fig.7 shows the GM and WM volumes of the brains of 13 subjects using CLASSIC and FANTASM. Fig.8 gives similar plots calculated within a local spherical region

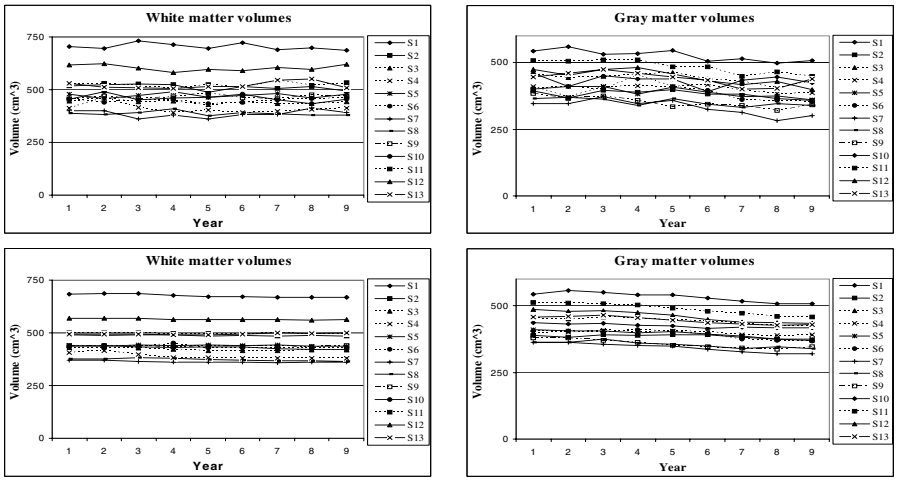

Fig. 7. GM and WM volumes of entire brains. Top: FANTASM, bottom: CLASSIC

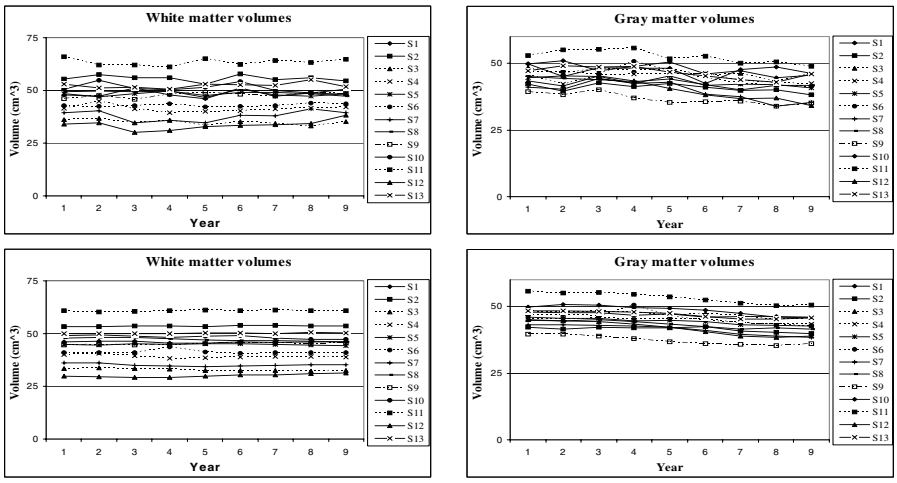

Fig. 8. GM and WM volumes in a local sphere. Top: FANTASM, bottom: CLASSIC

(see Fig.6). It can be seen that the curves of CLASSIC are quite smooth. Moreover, the GM and WM volumes calculated from the results of CLASSIC steadily decrease with time, which suggests tissue loss with aging. Although longitudinal analysis of MR brain images is much more complex, the experiments indicate that CLASSIC is a promising tool for longitudinally-consistent segmentation without compromising measurement of longitudinal atrophy.

4 Conclusion

We proposed an algorithm for segmentation of serial MR brain images, which yields spatially-adaptive and temporally-consistent segmentation results. The longitudinal deformations among the image series that reflect the underlying structural changes across time are also estimated. Experiments with simulated and real longitudinal MR brain images have confirmed the advantages of CLASSIC over more conventional 3-D segmentation analogous formulation.

References

1. Bezdek, J., Hall, L., Clarke, L.: Review of MR image segmentation techniques using pattern recognition. Medical Physics **20** (1993) 1033–1048
2. Pappas, T.: An adaptive clustering algorithm for image segmentation. IEEE Trans. on Signal Processing **40** (1992) 901–914
3. Udupa, J., Samarasekera, S.: Fuzzy connectedness and object definition: theory, algorithms and applications in image segmentation. Graph. Models Images Processing **58** (1996) 246–261
4. Brandt, M., Bohan, T., Kranmer, L., Fletcher, J.: Estimation of CSF, white and gray matter volumes in hydrocephalic children using fuzzy clustering of MR images. Comput. Med. Imag. Graph. **18** (1994) 25–34
5. Lim, K., Prefferbaum, A.: Segmentation of MR brain images into cerebrospinal fluid, white and gray matter. Journal of Comput. Assisted Tomogr. **13** (1989) 588–593
6. Pham, D., Prince, J.: Adaptive fuzzy segmentation of magnetic resonance images. IEEE Trans. on Medical Imaging **18** (1999) 737–752
7. Chen, W., Giger, M.: A fuzzy c-mean (FCM) based algorithm for intensity inhomogeneity correction and segmentation of MR images. In: IEEE International Symposium on Biomedical Imaging (ISBI 2004), Arlington, VA (2004) 1307–1310
8. Rezaee, M., van der Zwet, P., , Lelieveldt, B., van der Geest, R., Reiber, J.: A multiresolution image segmentation technique based on pyramidal segmentation and fuzzy clustering. IEEE Trans. on Image Processing **9** (2000) 1238–1248
9. Resnick, S., Goldszal, A., Davatzikos, C., Golski, S., Kraut, M., Metter, E., Bryan, R., Zonderman, A.: One-year age changes in MRI brain volumes in older adults. Cerebral Cortex **10** (2000) 464–472
10. Bezdek, J., Ehrlich, R., Full, W.: FCM: the fuzzy c-means clustering algorithm. Computers and Geosciences **10** (1984) 191–203
11. Guillemaud, R., Brady, M.: Estimating the bias field of MR images. IEEE Trans. on Medical Imaging **20** (1998) 57–68
12. Ahmed, M., Yamany, S., Mohamed, N., Farag, A., Moriarty, T.: A modified fuzzy c-means algorithm for bias field estimation and segmentation of MRI data. IEEE Trans. on Medical Imaging **21** (2002) 193–199
13. Liew, A., Leung, S., Lau, W.: Fuzzy image clustering incorporating spatial continuity. IEE Proc. Vis. Image Signal Process. **147** (2000) 185–192
14. Pham, D.: Spatial model for fuzzy clustering. Computer Vision and Image Understanding **84** (2001) 285–297
15. Shen, D., Davatzikos, C.: Measuring temporal morphological changes robustly in brain MR images via 4-D template warping. NeuroImage **21** (2004) 1508–1517

16. Shen, D., Davatzikos, C.: HAMMER: Hierarchical attribute matching mechanism for elastic registration. IEEE Trans. on Medical Imaging **21** (2002) 1421–1439
17. Nyul, G., Udupa, J., Zhang, X.: New variants of a method of MRI scale standardization. IEEE Trans. on Medical Imaging **19** (2000) 143–150
18. Zhu, C., Liu, F., Zhu, L., Jiang, T.: Anatomy dependent multi-context fuzzy clustering for separation of brain tissues in mr images. In: 2nd International Workshop on Medial Imaging and Augmented Reality, China (2004) 197–203
19. Karacali, B., Davatzikos, C.: Simulation of tissue atrophy using a topology preserving transformation model. Submit to IEEE Trans. on Medical Imaging (2004)